Engineering entanglement Hamiltonians with strongly interacting cold atoms in optical traps

R. E. Barfknecht,[1,2,*] T. Mendes-Santos,[3] and L. Fallani[4,2,1]

[1]*INO-CNR Istituto Nazionale di Ottica del CNR, Sezione di Sesto Fiorentino, 50019 Sesto Fiorentino, Italy*
[2]*LENS, European Laboratory for Non-Linear Spectroscopy, 50019 Sesto Fiorentino, Italy*
[3]*Abdus Salam International Centre for Theoretical Physics, Strada Costiera 11, 34151 Trieste, Italy*
[4]*Department of Physics and Astronomy, University of Florence, 50019 Sesto Fiorentino, Italy*

(Received 22 July 2020; accepted 14 January 2021; published 5 February 2021)

We present a proposal for the realization of entanglement Hamiltonians in one-dimensional critical spin systems with strongly interacting cold atoms. Our approach is based on the notion that the entanglement spectrum of such systems can be realized with a physical Hamiltonian containing a set of position-dependent couplings. We focus on reproducing the universal ratios of the entanglement spectrum for systems in two different geometries: a harmonic trap, which corresponds to a partition embedded in an infinite system, and a linear potential, which reproduces the properties of a half partition with open boundary conditions. Our results demonstrate the possibility of measuring the entanglement spectra of the Heisenberg and XX models in a realistic cold-atom experimental setting by simply using gravity and standard trapping techniques.

DOI: 10.1103/PhysRevResearch.3.013112

I. INTRODUCTION

The study of entanglement in quantum many-body systems [1,2] has become one of the major efforts in the physics community, not only because it is a central feature of quantum theories, but also due to its potential for describing quantum phases of matter and topological order [3–9]. Directly measuring entanglement, on the other hand, has proven to be a challenging task. This is due, in particular, to the difficulty of obtaining the full-state tomography [10] of many-body systems. Nevertheless, outstanding progress has been recently made with respect to the extraction of the entanglement properties of quantum systems, both in terms of theory [11–18] and experiments [19–22]. In common, these works feature indirect measurement protocols, either through the probing of correlations or by interference of identical copies of a system.

It is thus desirable to have at hand alternative proposals [23] for the measurement of entanglement that are at the same time direct—addressing quantities which are ordinarily accessible in experiments—and scalable. A significant step in this direction has been taken recently [24–27], with works showing that the entanglement spectrum [28,29] of lattice Hamiltonians can be reproduced by obtaining the physical spectrum of a Hamiltonian with the same general properties but with a set of spatially varying coupling parameters. This notion is based on the Bisognano-Wichmann (BW) theorem, which originally describes entanglement Hamiltonians for continuous systems in quantum field theory [30,31]. Later developments have shown [32] that features of the original model, such as boundary conditions, have a direct effect on the form of the couplings in the physical Hamiltonian. Such a relation hints at the prospect of reproducing the entanglement of discrete systems with Hamiltonians with specifically designed nonhomogeneous couplings.

In this context, an immediate possibility is the simulation of entanglement Hamiltonians with trapped systems of cold atoms [33], where optical confinement, atomic interactions, and internal states can be manipulated with remarkable precision [34–37]. On the theoretical side, it has been demonstrated that if the interactions between atoms are strong enough, the system can be mapped from the continuum to a spin chain, where the coupling coefficients are determined by the trapping geometry [38–41]. Experimentally, the strongly correlated regime is accessible with cold atoms both in fermionic [42–46] and bosonic [47–51] gases. The validity of the theoretical approach described above has also been verified in recent experiments [52].

Inspired by this perspective, in this article we show how to engineer the entanglement Hamiltonians of spin systems, such as the Heisenberg (XXX) and XX models, by considering a strongly interacting two-component system of cold atoms in effectively one-dimensional optical traps. Our first application is the case of harmonically trapped atoms giving rise to a spin chain where the couplings follow a parabolic distribution. As we will show, this remarkably ordinary assumption is enough to reproduce the universal ratios of the entanglement spectrum of a partition embedded in an infinite system with periodic boundary conditions. The second application assumes the presence of a linear potential, which in turn results in a set of linearly increasing couplings for the spin chain. In this regime, the physical Hamiltonian can reproduce the ratios of the entanglement spectrum of a half partition of a spin system

*barfknecht@lens.unifi.it

with open boundary conditions. The simple linear form of the potential additionally poses the intriguing possibility of using gravity as a tool for probing entanglement. To account for other experimental-related aspects, we also include density matrix renormalization group (DMRG) simulations of the continuum away from the strongly interacting limit, as well as the expected effect of finite temperatures on measurable quantities such as the dynamical structure factor.

II. SYSTEM DESCRIPTION

We calculate the entanglement properties of one-dimensional spin chains such as the Heisenberg model, $H_S = J\sum_{i=1}^{N-1} \boldsymbol{\sigma}_i \cdot \boldsymbol{\sigma}_{i+1}$, and the XX model, $H_S = J\sum_{i=1}^{N-1} \sigma_i^x\sigma_{i+1}^x + \sigma_i^y\sigma_{i+1}^y$, where $\boldsymbol{\sigma}$ denotes the Pauli vector and J is a homogeneous coupling. In the following, L denotes the total size of these homogeneous systems. After finding the ground-state solution $|\Psi\rangle$ for one of these models, the reduced density matrix for a subsystem A can be calculated by tracing over the remaining subsystem B with $\rho_A = \mathrm{Tr}_B|\Psi\rangle\langle\Psi| = e^{-H_A}/Z_A$, where H_A is called the *entanglement Hamiltonian* and Z_A is a normalization constant. The entanglement spectrum for partition A is then obtained as the set of eigenvalues $\{\epsilon_n\} = -\ln\{\epsilon_n^A\}$, where ϵ_n^A denotes the eigenvalues of the reduced density matrix.

The BW theorem for discrete systems [25] states that the entanglement Hamiltonian H_A can be equivalently calculated as $H_A \propto \sum_i J_i\boldsymbol{\sigma}_i \cdot \boldsymbol{\sigma}_{i+1}$, where J_i is a set of position-dependent couplings. Remarkably, results from conformal field theory predict [32,53] that these couplings should be given by

$$J_i \propto \frac{i(N-i)}{N} \quad \text{and} \quad J_i \propto i \tag{1}$$

for entanglement Hamiltonians corresponding to partitions embedded in an infinite system with periodic boundary conditions (which we label T_1) and half partitions in systems with open boundary conditions (T_2), respectively (see Fig. 1). More rigorously, for finite T_2 partitions, we have $J_i \propto \sin(\frac{\pi i}{2L})$; in Appendix B we investigate the role of finite-size effects in the results for systems with open boundary conditions (these are expected to scale to zero in the lower part of the energy spectrum as $L \to \infty$ [32]).

The results in Eq. (1) indicate that the entanglement Hamiltonians of spin systems can be simulated by constructing a *physical* Hamiltonian with a set of properly engineered couplings. A suitable platform for such an endeavor is an effectively one-dimensional cold atomic gas with a Hamiltonian described by $H_C = \sum_{i=1}^{N}(-\frac{1}{2}\frac{\partial^2}{\partial x_i^2} + V(x)) + g\sum_i^{N_\uparrow}\sum_j^{N_\downarrow}\delta(x_{i,\uparrow} - x_{j,\downarrow})$, where the first term on the right-hand side includes the presence of a trapping potential $V(x)$ and the second term accounts for atomic contact interactions (we assume a two-component gas where the internal states are labeled as $\uparrow, \downarrow$). The strength of the interactions is set by the parameter g (in units of $\hbar^2/ml$ where l is the characteristic length of the system), and we initially consider the fermionic case where interactions between atoms in the same internal state are forbidden by the Pauli principle.

In the strongly repulsive limit ($g \gg 1$), the wave function of the system described above is given by $\Psi = \sum_k a_k P_k \Phi_0$,

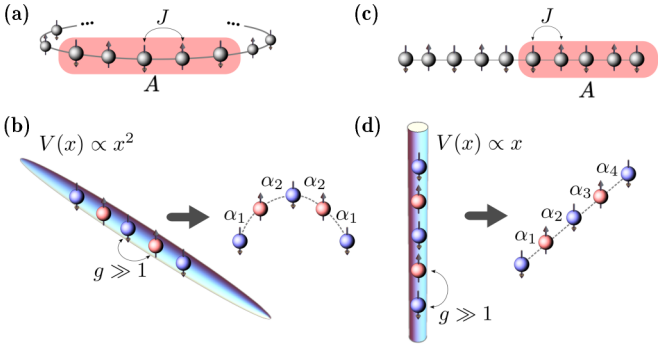

FIG. 1. (a) The entanglement spectrum of a partition embedded in an infinite spin system with periodic boundary conditions (T_1), which can be simulated with (b) a strongly interacting ($g \gg 1$) two-component system of cold atoms in a harmonic trap. We model this system as a spin chain where the exchange coefficients α_i follow the distribution of an inverted parabola. The entanglement spectrum of (c), a half partition of a finite spin chain with open boundary conditions (T_2) is reproduced with (d) a system of cold atoms in a linear potential, which can be realized by gravity. This system is mapped into a spin chain where the coefficients increase linearly with the position. The distribution of the coefficients can be very well approximated with the functions in Eq. (1). The antiferromagnetic order displayed in (b) and (d) corresponds to the ground state of Eq. (2) and is used for illustration purposes.

where $\Phi_0 = \Phi_0(x_{\uparrow 1}, ..., x_{\uparrow N_\uparrow}, x_{\downarrow 1}, ..., x_{\downarrow N_\downarrow})$ is the wave function in the limit of infinite repulsion and each term of the sum includes a permutation P_k (with amplitude a_k) of the coordinates. By employing the Hellmann-Feynman theorem along with boundary conditions for the contact interactions, H_c can be mapped into the following spin chain [39,54,55] (see Appendix A for details):

$$H = E_0 - \frac{1}{2}\sum_{i=1}^{N-1}\frac{\alpha_i}{g}(1 - \boldsymbol{\sigma}_i \cdot \boldsymbol{\sigma}_{i+1}), \tag{2}$$

where E_0 denotes the energy of the system at the fermionization limit where $g = \infty$. This mapping can be interpreted as a perturbation near the limit of infinite repulsion. (We can rewrite Eq. (2) in terms of the permutation operator $\Pi_{i,i+1} = \frac{1}{2}(1 + \boldsymbol{\sigma}_i \cdot \boldsymbol{\sigma}_{i+1})$ [39]). By diagonalizing this Hamiltonian we find the amplitudes a_k for the wave function Ψ and the energy spectrum in the limit of strong interactions. Another fundamental aspect of the approach described above is that, in Eq. (2), the position-dependent exchange coefficients α_i are obtained from the properties of the spatial wave function Φ_0 with $\alpha_i = \int_{x_1<\cdots<x_{N-1}} dx_1 \ldots dx_{N-1} |\frac{\partial\Phi_0}{\partial x_N}|^2_{x_N=x_i}$, which is independent of spin. The many-body wave function described by Φ_0 is constructed as the Slater determinant of the N lowest single-particle states in the trapping potential $V(x)$. In Eq. (2), the energy E_0 is simply given by the sum of the energies of each of these single-particle states. It is therefore clear that once we determine the geometry of the trap $V(x)$, we can obtain the exchange coefficients in Eq. (2). Calculating these integrals can be cumbersome for large N, but efficient methods which exploit the determinant properties of Φ_0 are available [56,57]. In Fig. 1 we show a sketch of the protocol adopted throughout this work.

We have thus established our proposal for simulating the entanglement spectrum of a spin chain with a two-component atomic system where the energy levels can be obtained by standard spectroscopy techniques [58]. The presence of strong interactions and trapping potentials not only allows for benchmarking the results against the limit of infinite repulsion, but also automatically generates the couplings needed for engineering entanglement Hamiltonians. The relation between entanglement and inhomogeneities in the underlying geometry of the system has been also explored, particularly for single-component systems, in Refs. [59–63].

III. RESULTS

To calculate the entanglement properties of the atomic systems described above, we start with the numerical values of the exchange coefficients α_i for a given trapping potential. We assume the cases of (a) a harmonic trap $V(x) = x^2/2$ and (b) a system confined by hard walls at $x = 0$ and $x = l$ and exposed to a linear potential $V(x) = V_0(l - x)$. The distribution of the coefficients in the harmonic trap is symmetric across the origin and has the shape of an inverted parabola [64,65]. For the tilted potential, we find that the coefficients increase linearly and are given by $\alpha_i = V_0 i$ (see sketch in Fig. 1). In Appendix B we show a comparison with these results with a fit of the functions in Eq. (1).

We can now compare the entanglement spectrum of a physical Hamiltonian with spatially varying couplings and the exact results for different partitions. For the Heisenberg model, the physical Hamiltonian is given by Eq. (2). The XX model can analogously by reproduced by initially considering a bosonic system in the continuum, where interaction between atoms in the same internal states are allowed. This results in an additional term in Eq. (2) given by $-\frac{1}{2}\sum_{i=1}^{N-1}\frac{\alpha_i}{g'}(1+\sigma_i^z\sigma_{i+1}^z)$, where g' denotes the interspecies interactions [54]. Our focus is on obtaining universal ratios for the entanglement spectrum, defined as $\kappa_n = |\frac{\epsilon_n-\epsilon_1}{\epsilon_r-\epsilon_1}|$, where n denotes the energy level, ϵ_1 is the ground-state energy, and ϵ_r is a reference level (unless stated otherwise, we fix $r = 3$—the second excited state). We point out that the specific magnetic correlations of each state, including the ground state of a particular model, are not relevant for this calculation.

In Figs. 2(a) and 2(d) we show the results for this quantity obtained by exact diagonalization. The physical spectrum of the harmonically trapped, strongly interacting Hamiltonian is compared to a partition embedded in a system with periodic boundary conditions, while the case of a linear potential is compared to a half partition of the same size in a system with open boundary conditions. Additionally, we include the results for an "ideal" physical Hamiltonian with a set of couplings provided by Eq. (1). The agreement between the results obtained with three different approaches is particularly remarkable for small values of n, corresponding to the low-energy part of the entanglement spectrum. The discrepancy with the exact results obtained from the reduced density matrix (black solid curves) at higher energies stems mainly from finite-size effects.

In Figs. 2(e) and 2(f), we include also results obtained with DMRG, where we see that the agreement between the entanglement spectrum of homogeneous partitions of the Heisenberg model and the physical spectrum of trapped fermions also holds for larger systems.

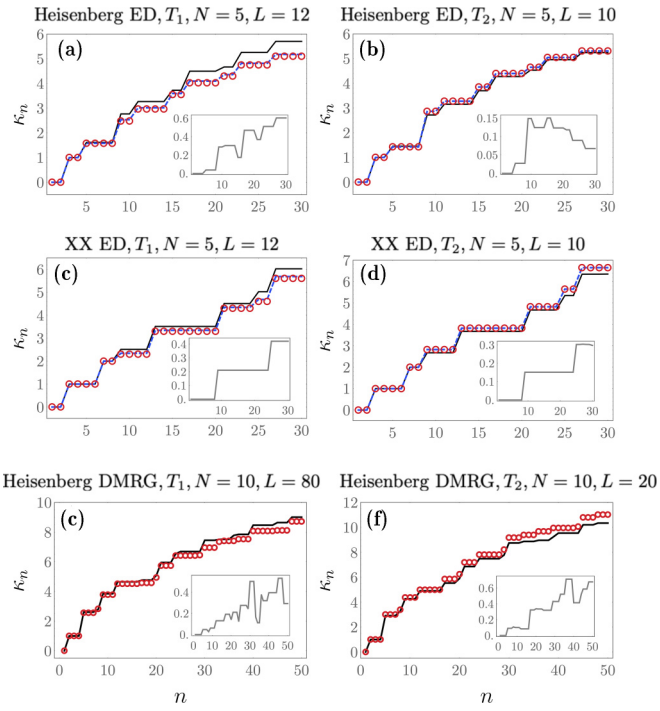

FIG. 2. Comparison of the universal ratios κ_n for the (a), (b) Heisenberg and (c), (d) XX models with $N = 5$. The left column show the results for partitions T_1 (black solid lines, total size of the system $L = 12$), compared to the case of harmonically trapped atoms (red circles). The right column show the analog results for partitions T_2 (total size of the system $L = 10$) and atoms in a linear potential. In the first four panels we additionally include the results for a Hamiltonian with $N = 5$ and a set of ideal couplings given by Eq. (1) (blue dashed lines). In (e), (f) we present the results for the Heisenberg model with larger size ($N = 10$). The results for the partitions are obtained with DMRG for systems of total size (e) $L = 80$ and $L = 20$, respectively. The interaction strength for the trapped atoms is set as $g = 20$ (in units of $\hbar^2/ml$). In all plots, the insets show the absolute numerical difference between the red circles and the black lines.

IV. EXPERIMENTAL DETAILS

Effectively one-dimensional systems of cold atoms are currently realized in the laboratory by loading the atoms into tight optical waveguides, where the confinement along the transverse direction is much larger than the longitudinal one. These waveguides can be provided by optical lattices, where the transverse confinement could easily reach values on the order of $\omega_\perp = 2\pi 50$ kHz, with $\hbar\omega_\perp$ much larger than temperature and atomic chemical potential.

Different spin states can be simulated by exploring the internal degrees of freedom of particular atomic species. Usually, these are hyperfine states in alkali elements (such as fermionic ^{6}Li and bosonic ^{87}Rb), but nuclear-spin states in alkaline-earth elements like ^{173}Yb or ^{87}Sr can also be used.

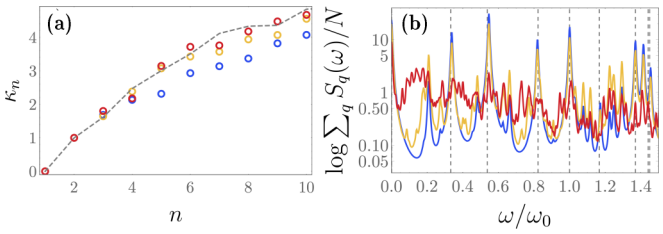

FIG. 3. (a) Comparison of the universal ratios of the Heisenberg model with the ideal coefficients in Eq. (1) (gray dashed curves) to DMRG simulations of the continuum for fermions in a harmonic trap. Blue, yellow, and red circles correspond to interaction strength $g = 5, 10$, and 15 (in units of $\hbar^2/ml$), respectively. The universal ratios κ_n are calculated having as a reference state $r = 2$. (b) Temperature-dependent dynamical structure factor (summed over q) for harmonically trapped fermions [Eq. (2)] with $g = 25$. Blue, yellow, and red curves correspond $k_BT \approx 0.008\epsilon_F$, $0.2\epsilon_F$, and $0.8\epsilon_F$, respectively, where ϵ_F is the Fermi energy of a system of spinless fermions with the same number of particles. The vertical gray dashed lines denote the position of the energy gaps corresponding to the universal ratios obtained for the Heisenberg model with couplings given by Eq. (1). The reference state for these calculations is $r = 4$, and the frequency ω_0 is analogously defined as $\omega_0 = (\epsilon_4 - \epsilon_0)/\hbar$. In both panels, we assume $N = 7$ in a sector of fixed magnetization $+1/2$.

These last cases also provide the opportunity of exploring additional internal states with SU(N) symmetry [45,66].

With state-of-the-art atom trapping techniques there are ample possibilities of controlling the potential parameters to engineer the required exchange coupling α_i. Typical axial harmonic trapping frequencies for the scenario shown in Fig. 1(b) lie in the range $\omega_T = 2\pi(10\text{–}10^3)$ Hz. The protocol shown in Fig. 1(d) can be realized either by means of magnetic and/or optical gradients or by exploiting the effect of gravity, where the linear potential could be tuned by changing the tilting angle of the tubes. An additional focused laser beam (or other spatial-light-modulator-based techniques) is required to create hard walls at the bottom of the tubes for keeping the atoms confined.

We also address here experimental aspects which can be relevant in the detection of the physical spectrum of trapped systems: finiteness of interactions and temperature. To investigate the first, we realize simulations of the continuum with the Hubbard model in an underlying harmonic trap. In Fig. 3(a) we show a comparison of the universal ratios obtained with this approach to the expected results for a Heisenberg model with a set of coefficients given by Eq. (1). We find that even at a moderate interaction regime (well within the experimental capabilities) the measured spectrum agrees with the entanglement spectrum of the target model (especially at small n). This calculation also provides an independent check of the validity of the spin-mapping approach described in the main part of this paper. In experiments, interactions between atoms can be manipulated by means of Feshbach [67] or confinement induced resonances [68]. In the strongly interacting regime, such systems may suffer from losses due to three-body recombination; however, in the fermionic case this effect is suppressed by the Pauli exclusion principle, which increases the lifetime of the experiment. The effect of temperature is now quantified by calculating the temperature-dependent dynamical structure factor [69–71] $S(q,\omega) = Z(T)^{-1}\sum_{i,j} e^{(-E_i/k_BT)}|\langle i|S^z_q|j\rangle|^2\delta[\omega - (E_i - E_j)]$, where $Z(T) = \mathrm{Tr}(e^{-H/k_BT})$ is the canonical partition function, k_B is the Boltzmann constant, and $|i\rangle$ and $|j\rangle$ denote the eigenstates; $S^z_q = \sum_i \sqrt{(2)}\sin(qi)S^z_i/\sqrt{(N+1)}$ is the Fourier transform of the operator $S^z_i = \sigma^z_i/2$ and $q = n\pi/(N+1)$. In Fig. 3(b) we compare the excitation spectrum of the dynamical structure factor (at values of k_BT corresponding to different fractions of the Fermi energy for a system of spinless fermions, denoted by ϵ_F) to the position of the energy gaps corresponding to the universal ratios. Particularly, at lower temperatures we find pronounced peaks located precisely at the energy values predicted with κ_n that are clearly visible for experimentally achievable temperatures $k_BT \approx 0.2\epsilon_F$ (note the vertical logarithmic scale). As expected, for larger temperatures such results are washed out by the contribution of several additional frequencies.

In these calculations, we have assumed that the system has a fixed total magnetization; to obtain results such as the ones shown in Fig. 2 in an experiment, a number of measurements would be performed, each in different magnetization sectors (from the fully polarized to the completely balanced spin combinations). Measurements of the structure factor could be carried out by performing Bragg spectroscopy. We find that the frequencies shown in Fig. 3 are well within reach of the typical lifetimes of experiments with cold fermions. As a matter of fact, for realistic trapping frequencies of the order of $\omega = 2\pi \times 200$ Hz, the energy scale of the resonances in Fig. 3(b) is $\omega_0 \sim 80$ Hz. In experiments with two-component 1D fermions, in the strongly repulsive regime lifetimes on the order of $\tau \sim 1$ s have already been measured [72], enabling a Fourier-limited frequency resolution on the order of $\tau^{-1} \sim 1$ Hz, which is one order of magnitude better than the features of the spectrum we are interested to resolve.

V. CONCLUSIONS

We have presented a theoretical proposal for the realization of entanglement Hamiltonians with strongly interacting cold atoms in effectively one-dimensional optical traps. A key feature of these models is the possibility of mapping the Hamiltonian into a spin chain with a set of couplings that depend on the underlying geometry. By simply assuming a harmonic confinement, we have shown that the universal ratios of the entanglement for a partition embedded in an infinite system can be reproduced. Analogously, a linear potential can produce the results expected for a half partition in a finite system. The energy spectrum of these systems can be obtained by standard spectroscopy of cold atoms in elongated harmonic traps or boxlike traps under the effect of gravity. We have benchmarked our predictions against important experimental effects such as finite interaction strength and temperature, evidencing the experimental feasibility of our proposal. Such a protocol can be extended to the study of various spin Hamiltonians, like systems with higher internal symmetries [73]; in such cases, the particular details (e.g., interactions and internal states) of a given atomic model will determine the structure of

the spin chain [74,75]. Nevertheless, the relation between the couplings and the geometry of the external trap remains valid in the limit of strong interactions.

ACKNOWLEDGMENTS

The authors thank Marcello Dalmonte for discussing the project and for valuable comments on the manuscript. Jacopo Catani is acknowledged for important remarks on the experimental feasibility of the proposal. We acknowledge support from the European Research Council (ERC Consolidator Grant TOPSIM, Grant Agreement No. 682629), European QuantERA ERA-NET Cofund in Quantum Technologies (Project QTFLAG, Grant Agreement No. 731473), Ministero dell'Istruzione, dell'Università e della Ricerca (MIUR Project FARE TOPSPACE R16SPCCRCW, and MIUR PRIN Project No. 2017E44HRF). The DMRG calculations shown in this paper were performed using the ITensor library [76].

APPENDIX A: MAPPING A STRONGLY INTERACTING ATOMIC SYSTEM TO A SPIN CHAIN

The general procedure described in this section has been developed and extensively detailed in different works, such as Refs. [38–40]. Further discussions and applications to different atomic models can be found, for instance, in Refs. [41,74]. Below we reproduce the essential steps required to obtain the spin chain models considered in the main text. We start by considering a one-dimensional two-component fermionic system with contact interactions, described by

$$H = \sum_{i=1}^{N} H_0(x_i) + g \sum_{i=1}^{N_\uparrow} \sum_{j=1}^{N_\downarrow} \delta(x_{\uparrow i} - x_{\downarrow j}), \tag{A1}$$

where $N = N_\uparrow + N_\downarrow$. In the limit of infinite repulsion ($g \to \infty$), we can write the complete many-body wave function as

$$\Psi = \sum_{k=1}^{L(N_\uparrow, N_\downarrow)} a_k P_k \Phi_0(\{x_{\uparrow i}, x_{\downarrow j}\}), \tag{A2}$$

where P_k is the permutation operator, and the sum is carried over a total number of $L(N_\uparrow, N_\downarrow) = \binom{N_\uparrow + N_\downarrow}{N_\uparrow}$ permutations. In this context Φ_0 is the wave function in the limit of infinite repulsion where $\{x_{\uparrow i}, x_{\downarrow j}\}$ denotes a given ordering of the particles.

For strong finite interactions, the Hellmann-Feynman theorem can be employed to write

$$\frac{\partial E}{\partial g} = \sum_{i=1}^{N_\uparrow} \sum_{j=1}^{N_\downarrow} \langle \Psi | \delta(x_{\uparrow i} - x_{\downarrow j}) | \Psi \rangle. \tag{A3}$$

Additionally, we write the expression for the derivative condition at the contact point between particles as

$$\left(\frac{\partial \Psi}{\partial x_{\uparrow i}} - \frac{\partial \Psi}{\partial x_{\downarrow j}} \right) \Bigg|_{x_{\uparrow i} - x_{\downarrow j} = 0^-}^{x_{\uparrow i} - x_{\downarrow j} = 0^+} = 2g\Psi(x_{\uparrow i} = x_{\downarrow j}), \tag{A4}$$

which follows the standard procedure of the coordinate Bethe ansatz approach [77]. Plugging Eq. (A4) into Eq. (A3) and integrating with respect to g, we find

$$E = E_0 - \frac{\sum_{i=1,j=1}^{N_\uparrow, N_\downarrow} \int dx_{\uparrow 1}, \ldots, dx_{\uparrow N_\uparrow} \int dx_{\downarrow 1}, \ldots, dx_{\downarrow N_\downarrow} \left| \left(\frac{\partial \Psi}{\partial x_{\uparrow i}} - \frac{\partial \Psi}{\partial x_{\downarrow j}} \right) \right|_{x_{\uparrow i} - x_{\downarrow j} = 0^-}^{x_{\uparrow i} - x_{\downarrow j} = 0^+}{}^2 \delta(x_{\uparrow i} - x_{\downarrow j})}{4g \int dx_{\uparrow 1}, \ldots, dx_{\uparrow N_\uparrow} \int dx_{\downarrow 1}, \ldots, dx_{\downarrow N_\downarrow} |\Psi|^2}, \tag{A5}$$

where we discard terms of order $O(1/g^2)$ and higher. In this expression, E_0 denotes the energy of a system of spinless fermions (which is the same energy expected in the regime of infinite repulsion). By inserting (A2) in this equation, we find

$$E = E_0 - \frac{\sum_{i=1}^{N-1} \frac{\alpha_i}{g} \sum_{k=1}^{L(N_\uparrow - 1, N_\downarrow - 1)} (a_{ik} - a'_{ik})^2}{\sum_{k=1}^{L(N_\uparrow, N_\downarrow)} a_k^2}, \tag{A6}$$

where a_{ik} denotes the wave-function coefficient where neighboring $\uparrow$ and $\downarrow$ fermions are found in positions i and $i+1$, while a'_{ik} is the coefficient for the wave function where the particle positions are $i+1$ and i. In this expression, we have

$$\alpha_i = \frac{\int_{x_1 < x_2 \cdots < x_N - 1} dx_1 \ldots dx_{N-1} \left| \frac{\partial \Phi_0(x_1, \ldots, x_i, \ldots, x_N)}{\partial x_N} \right|^2_{x_N = x_i}}{\int_{x_1 < x_2 \cdots < x_N - 1} dx_1 \ldots dx_N |\Phi_0(x_1, \ldots, x_i, \ldots, x_N)|^2}, \tag{A7}$$

which is not spin dependent. Thus Φ_0 can now be treated as the wave function for a system of spinless fermions.

We now take under consideration a spin Hamiltonian given by

$$H = E_0 - \sum_{i=1}^{N-1} J_i \Pi_{i,i+1}, \tag{A8}$$

where $\Pi_{\uparrow\downarrow}^{i,i+1} = \frac{1}{2}(1 - \boldsymbol{\sigma}_i \cdot \boldsymbol{\sigma}_{i+1})$ is the permutation operator. A general wave function for this Hamiltonian can be written as

$$|\chi\rangle = \sum_{k=1}^{L(N_\uparrow, N_\downarrow)} a_k P_k |\uparrow_1 \cdots \uparrow_{N_\uparrow} \downarrow_1 \cdots \downarrow_{N_\downarrow}\rangle, \tag{A9}$$

in analogy with Eq. (A2). Using this wave function, we calculate $\langle \chi | H | \chi \rangle$ as

$$\langle \chi | H | \chi \rangle = E_0 - \frac{\sum_{i=1}^{N-1} J_i \sum_{k=1}^{L(N_\uparrow - 1, N_\downarrow - 1)} (a_{ik} - a'_{ik})^2}{\sum_{k=1}^{L(N_\uparrow, N_\downarrow)} a_k^2}, \tag{A10}$$

where a_{ik} and a'_{ik} are as described for Eq. (A6). This means that expressions (A6) and (A10) are equivalent provided that

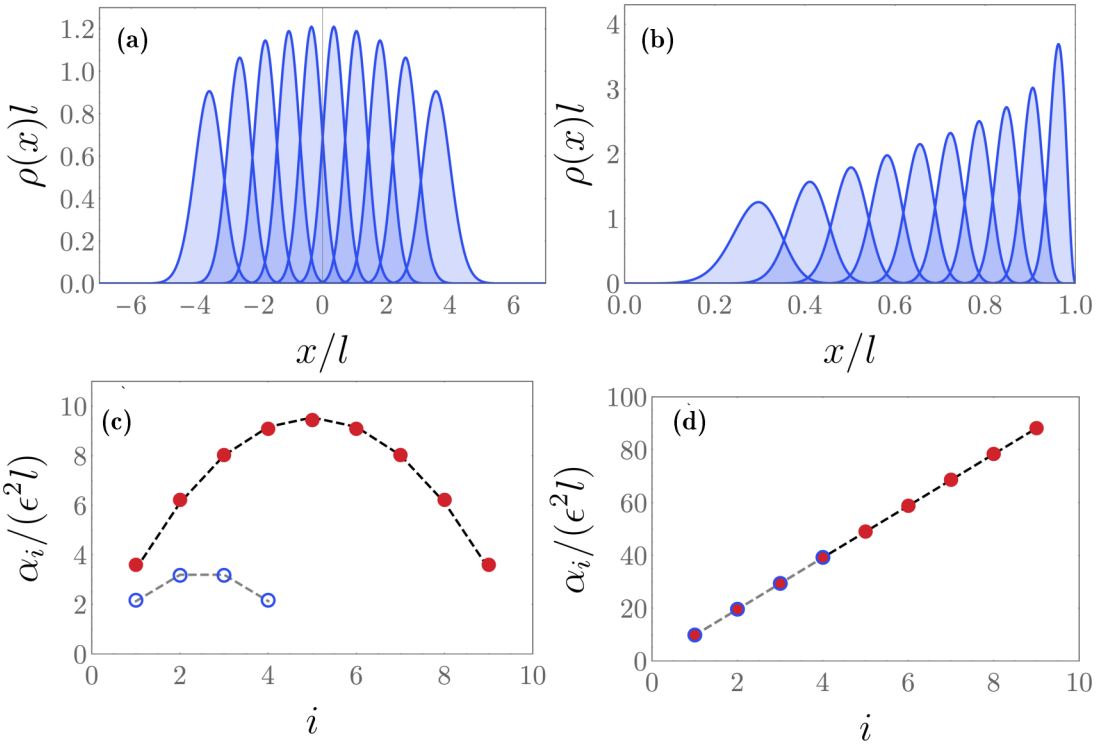

FIG. 4. (a), (b) Spatial distributions for $N = 10$ spinless fermions in the cases of (a) the harmonic trap and (b) a finite system of length l with a linear potential. The total density in each case is normalized to the total number of particles N. (c), (d) Numerical values of the exchange coefficients for the (a) harmonic trap and (b) the linear trap. The red dots indicate the results for $N = 10$, while the blue circles show results for $N = 5$. The black and gray dashed curves display results for the fits obtained with Eq. (1) of the main text.

$J_i = \alpha_i/g$. We can now rewrite Eq. (A8) as

$$H = E_0 - \frac{1}{2}\sum_{i=1}^{N-1}\frac{\alpha_i}{g}(1 - \boldsymbol{\sigma}_i \cdot \boldsymbol{\sigma}_{i+1}), \tag{A11}$$

which is the Hamiltonian given in Eq. (2).

APPENDIX B: ADDITIONAL RESULTS AND DETAILS ON THE SIMULATIONS

1. Particle densities and exchange coefficients

In the main text, we employ the exchange coefficients of a spin chain describing a system of strongly interacting trapped atoms to calculate the entanglement spectrum of homogeneous spin partitions. Below we present the results for the spatial distributions of the atoms in the trap and the values of the coefficients. The densities are calculated with the following expression:

$$\rho^i(x) = \int_\Gamma dx_1 ... dx_N\, \delta(x_i - x)|\Phi_0(x_1, ..., x_i, ..., x_N)|^2, \tag{B1}$$

where the integration is restricted to the sector $\Gamma = x_1 < x_2 < \cdots < x_N$. For larger systems, it is convenient to explore the determinant properties of the wave function Φ_0 [78] and write

$$\rho^i(x) = \frac{\partial}{\partial x}\left(\sum_{j=0}^{N-1}\frac{(-1)^{N-1}(N-j-1)!}{(i-1)!(N-j-i)!j!}\frac{\partial^j}{\partial\lambda^j}\det\left[B(x) - 1\lambda\right]|_{\lambda=0}\right), \tag{B2}$$

where the elements of the matrix $B(x)$ are written as $b_{mn}(x) = \int_{-\infty}^{x} dy\, \varphi_m(y)\varphi_n(y)$, and $\varphi(x)$ denotes the single-particle states in a corresponding trapping potential. For the simple case of the harmonic trap, these can be obtained exactly; for the linear potential, we obtain the single-particle solutions by numerical diagonalization, using as a basis 50 eigenstates of the box potential. The characteristic length l in the harmonic trap is related to the trapping frequency ω by $l = \sqrt{\hbar/m\omega}$ (we assume $\omega = 1$ in our calculations). In Figs. 4(a) and 4(b), we show the spatial densities of $N = 10$ spinless fermions obtained with Eq. (B2) for the harmonic trap an the linear potential, respectively. Due to the Bose-Fermi mapping theorem, these distributions are identical to those of a infinitely repulsive bosonic system, namely, the Tonks-Girardeau gas, in the same trapping potential [79]. In Figs. 4(c) and 4(d), we show the results for the exchange coefficients in each trapping potential. By comparing with (a) and (b), it becomes clear that the particle overlaps to determine the numerical values of the

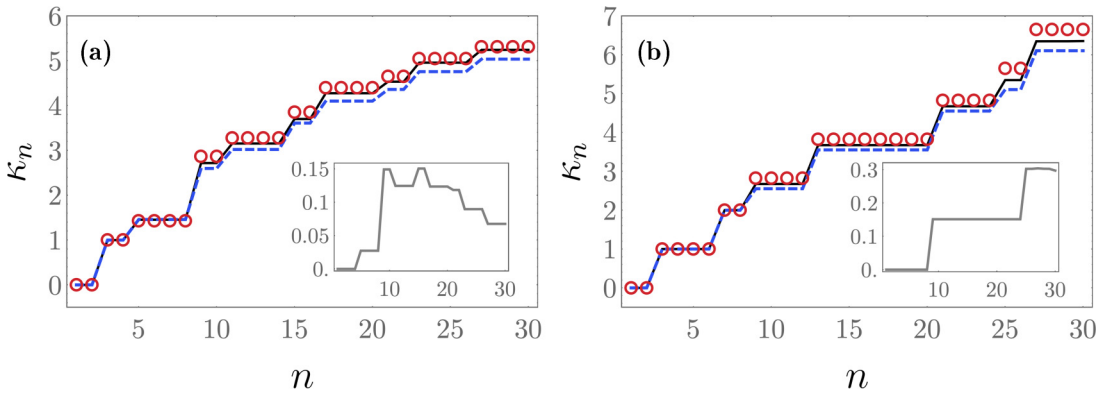

FIG. 5. Comparison of the results of the entanglement spectrum for (a) the Heisenberg and (b) XX models in partitions T_2 (black curves) with strongly interacting fermions in a linear potential (red circles) and Hamiltonians with the exact set of couplings for finite systems given by Eq. (B3) (blue dashed curves). The parameters assumed are the same as in Figs. 2(b) and 2(d) of the main text. The insets show the absolute numerical difference between the red circles and the black lines.

exchange coefficients α_i. In (c) and (d), we additionally show a comparison with the results obtained by fitting the functions in Eq. (1), which displays excellent agreement. We also show results for a system with $N = 5$ fermions. In these cases the coefficients can be calculated with the integrals provided in the main text. For larger systems we use the open-source program CONAN [56].

2. Entanglement spectrum

In Fig. 2 of the main text, the results for partitions of type T_2 are compared to the spectrum of a physical Hamiltonian where the coefficients follow the distribution given in Eq. (1), that is, $J_i \propto i$. However, strictly speaking, the coefficients for a half partition in a finite system with open boundary conditions have been shown to obey [32])

$$J_i = \frac{2L}{\pi} \sin\left(\frac{\pi i}{2L}\right). \tag{B3}$$

In Fig. 5 we show the results for the Heisenberg and XX models, where the results for a Hamiltonian with ideal couplings (blue dashed lines) are obtained with the exact results for finite systems. As expected, these show a slight discrepancy with respect to the results of atoms in a linear potential, especially at higher energies. Such discrepancies, however, should vanish as $L \to \infty$.

In Figs. 2(e) and 2(f) of the main text, we showed the comparison between the universal ratios obtained with ED for trapped atoms and DMRG for partitions embedded in larger systems, focusing on the Heisenberg model. Here we present in Fig. 6 also the case of the XX model, where the size of the system is the same as considered in the main text. The results corresponding to the XX model are obtained by assuming a bosonic strongly interacting system with $g' = 2g$ being the intraspecies interaction parameter.

3. DMRG details

In Figs. 2(e) and 2(f) of the main text and in Fig. 6 of this section, the black curves are calculated with DMRG simulations of the Heisenberg model [76], with a total of six sweeps and a maximum bond dimension of 600. In Fig. 4 of the

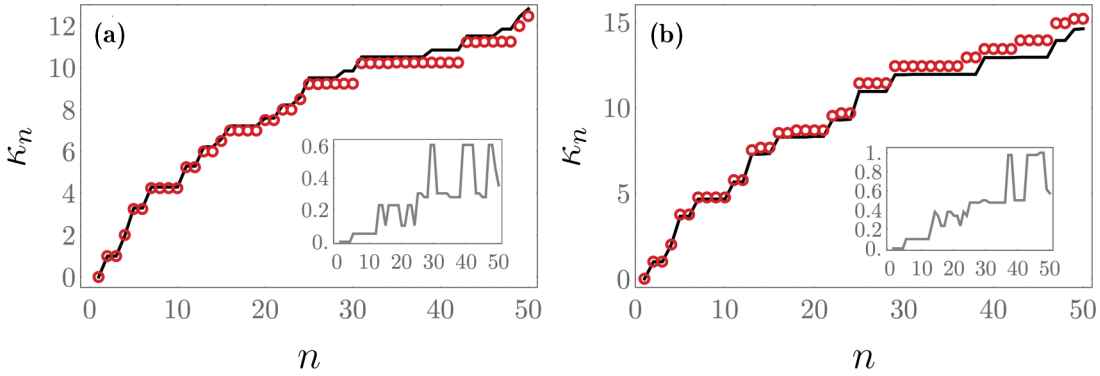

FIG. 6. Comparison of the universal ratios in the XX model for systems with $N = 10$ in the case of (a) the harmonic trap and (b) the linear potential. The results for the partitions with (a) periodic boundary conditions and (b) open boundary conditions (black curves) are obtained with DMRG for systems of total size $L = 80$ and $L = 20$, respectively. The interaction parameters for the trapped atomic system are set as $g = 20$ and $g' = 2g$ (see main text). The insets show the absolute numerical difference between the results.

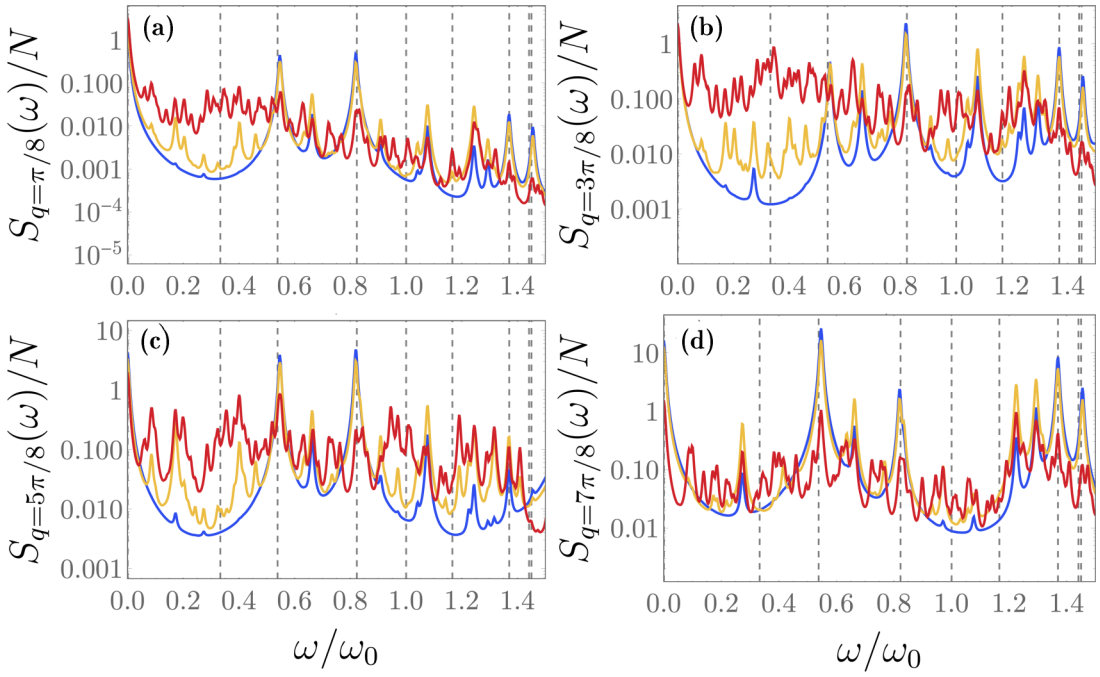

FIG. 7. Temperature-dependent dynamical structure factor for harmonically trapped fermions with $g = 25$ in the cases of (a) $q = \pi/8$, (b) $q = 3\pi/8$, (c) $5\pi/8$, and (d) $7\pi/8$. Blue, yellow, and red curves correspond $k_B T \approx 0.008\epsilon_F$, $0.2\epsilon_F$, and $0.8\epsilon_F$, respectively, where ϵ_F is the Fermi energy of a system of spinless fermions with the same number of particles. The vertical gray dashed lines denote the position of the energy gaps corresponding to the universal ratios obtained for the Heisenberg model with couplings given by Eq. (1). The reference states for these calculations is $r = 4$, and the frequency ω_0 is analogously defined as $\omega_0 = (\epsilon_4 - \epsilon_0)/\hbar$. We assume $N = 7$ in a sector of fixed magnetization $+1/2$.

main text, we calculate the universal ratios for a system of $N = 7$ trapped fermions with DMRG by approximating the continuum with the Hubbard model,

$$H = -t \sum_{j,\sigma} (c^{\dagger}_{j+1,\sigma} c_{j,\sigma} + \text{H.c.}) + U \sum_{j} n_{j,\uparrow} n_{j,\downarrow} + \sum_{j,\sigma} V_j n_{j,\sigma}, \tag{B4}$$

where the last term denotes the underlying harmonic trap potential. The simulation of the continuum is performed with a total of $N_s = 200$ Hubbard sites. By fixing a length λ we define the lattice spacing as $a = \lambda/N_s$. The hopping parameter is then related to the kinetic term in the continuum as $t = 1/(2a^2)$ (assuming $m = 1$), while the interaction parameters are related by $U = g/a$ [80]. In these simulations we perform a total of 40 DMRG sweeps, with a maximum bond dimension of 10^6. The maximum truncation error at the final sweep is $\sim 10^{-11}$.

4. Temperature-dependent dynamical structure factor

In the results contained in the main text for the temperature-dependent dynamical structure factor, we approximate the delta function $\delta[\omega - (E_i - E_j)]$ with a Lorentzian given by

$$f(\omega) = \frac{1}{\pi} \frac{\eta^2}{\eta^2 + \omega^2}, \tag{B5}$$

where $\eta = 0.002$. In Fig. 4(b) we summed over all values of momentum q. In Fig. 7 we also show the separate results for this quantity at particular momentum values. In all the results obtained for the structure factor, the frequencies are normalized by $\omega_0 = (\epsilon_4 - \epsilon_0)/\hbar$, where ϵ_0 and ϵ_4 are the ground state and fourth excited-state energies, respectively. It is worth estimating how the frequencies shown in Figs. 4(b) and 7 compare to the typical lifetimes of experiments with cold atoms. For fermions, these lifetimes can be of the order of a second, which allows for an experimental resolution of around 1 Hz. If we assume a harmonic trap with a realistic frequency of $\sim$200 Hz, we find a frequency gap of $\omega_0 \approx 80$ Hz, which is well within the reach of current experiments.

[1] L. Amico, R. Fazio, A. Osterloh, and V. Vedral, Entanglement in many-body systems, Rev. Mod. Phys. **80**, 517 (2008).
[2] R. Horodecki, P. Horodecki, M. Horodecki, and K. Horodecki, Quantum entanglement, Rev. Mod. Phys. **81**, 865 (2009).
[3] P. Calabrese and J. Cardy, Entanglement entropy and conformal field theory, J. Phys. A: Math. Theor. **42**, 504005 (2009).
[4] F. Pollmann, A. M. Turner, E. Berg, and M. Oshikawa, Entanglement spectrum of a topological phase in one dimension, Phys. Rev. B **81**, 064439 (2010).

[5] H. Li and F. D. M. Haldane, Entanglement Spectrum as a Generalization of Entanglement Entropy: Identification of Topological Order in Non-Abelian Fractional Quantum Hall Effect States, Phys. Rev. Lett. **101**, 010504 (2008).

[6] L. Fidkowski, Entanglement Spectrum of Topological Insulators and Superconductors, Phys. Rev. Lett. **104**, 130502 (2010).

[7] R. Thomale, A. Sterdyniak, N. Regnault, and B. A. Bernevig, Entanglement Gap and a New Principle of Adiabatic Continuity, Phys. Rev. Lett. **104**, 180502 (2010).

[8] X.-L. Qi, H. Katsura, and A. W. W. Ludwig, General Relationship between the Entanglement Spectrum and the Edge State Spectrum of Topological Quantum States, Phys. Rev. Lett. **108**, 196402 (2012).

[9] G. De Chiara, L. Lepori, M. Lewenstein, and A. Sanpera, Entanglement Spectrum, Critical Exponents, and Order Parameters in Quantum Spin Chains, Phys. Rev. Lett. **109**, 237208 (2012).

[10] M. E. Beverland, J. Haah, G. Alagic, G. K. Campbell, A. M. Rey, and A. V. Gorshkov, Spectrum Estimation of Density Operators with Alkaline-Earth Atoms, Phys. Rev. Lett. **120**, 025301 (2018).

[11] J. Cardy, Measuring Entanglement Using Quantum Quenches, Phys. Rev. Lett. **106**, 150404 (2011).

[12] C. M. Alves and D. Jaksch, Multipartite Entanglement Detection in Bosons, Phys. Rev. Lett. **93**, 110501 (2004).

[13] A. J. Daley, H. Pichler, J. Schachenmayer, and P. Zoller, Measuring Entanglement Growth in Quench Dynamics of Bosons in an Optical Lattice, Phys. Rev. Lett. **109**, 020505 (2012).

[14] D. A. Abanin and E. Demler, Measuring Entanglement Entropy of a Generic Many-Body System with a Quantum Switch, Phys. Rev. Lett. **109**, 020504 (2012).

[15] A. Elben, B. Vermersch, M. Dalmonte, J. I. Cirac, and P. Zoller, Rényi Entropies from Random Quenches in Atomic Hubbard and Spin Models, Phys. Rev. Lett. **120**, 050406 (2018).

[16] B. Vermersch, A. Elben, M. Dalmonte, J. I. Cirac, and P. Zoller, Unitary n-designs via random quenches in atomic Hubbard and spin models: Application to the measurement of Rényi entropies, Phys. Rev. A **97**, 023604 (2018).

[17] I. Morera, A. Polls, and B. Juliá-Díaz, Entanglement structure of the two-component Bose-Hubbard model as a quantum simulator of a Heisenberg chain, Sci. Rep. **9**, 9424 (2019).

[18] A. P. Tonel, L. H. Ymai, K. W. W., A. Foerster, and J. Links, Entangled states of dipolar bosons generated in a triple-well potential, SciPost Phys. Core **2**, 3 (2020).

[19] R. Islam, R. Ma, P. M. Preiss, M. Eric Tai, A. Lukin, M. Rispoli, and M. Greiner, Measuring entanglement entropy in a quantum many-body system, Nature (London) **528**, 77 (2015).

[20] T. Fukuhara, S. Hild, J. Zeiher, P. Schauß, I. Bloch, M. Endres, and C. Gross, Spatially Resolved Detection of a Spin-Entanglement Wave in a Bose-Hubbard Chain, Phys. Rev. Lett. **115**, 035302 (2015).

[21] P. Hauke, M. Heyl, L. Tagliacozzo, and P. Zoller, Measuring multipartite entanglement through dynamic susceptibilities, Nat. Phys. **12**, 778 (2016).

[22] T. Brydges, A. Elben, P. Jurcevic, B. Vermersch, C. Maier, B. P. Lanyon, P. Zoller, R. Blatt, and C. F. Roos, Probing Rényi entanglement entropy via randomized measurements, Science **364**, 260 (2019).

[23] H. Pichler, G. Zhu, A. Seif, P. Zoller, and M. Hafezi, Measurement Protocol for the Entanglement Spectrum of Cold Atoms, Phys. Rev. X **6**, 041033 (2016).

[24] J. Cardy and E. Tonni, Entanglement Hamiltonians in two-dimensional conformal field theory, J. Stat. Mech.: Theory Exp. (2016) 123103.

[25] M. Dalmonte, B. Vermersch, and P. Zoller, Quantum simulation and spectroscopy of entanglement Hamiltonians, Nat. Phys. **14**, 827 (2018).

[26] G. Giudici, T. Mendes-Santos, P. Calabrese, and M. Dalmonte, Entanglement Hamiltonians of lattice models via the Bisognano-Wichmann theorem, Phys. Rev. B **98**, 134403 (2018).

[27] T. Mendes-Santos, G. Giudici, R. Fazio, and M. Dalmonte, Measuring von Neumann entanglement entropies without wave functions, New J. Phys. **22**, 013044 (2020).

[28] P. Calabrese and A. Lefevre, Entanglement spectrum in one-dimensional systems, Phys. Rev. A **78**, 032329 (2008).

[29] A. Chandran, V. Khemani, and S. L. Sondhi, How Universal is the Entanglement Spectrum? Phys. Rev. Lett. **113**, 060501 (2014).

[30] J. J. Bisognano and E. H. Wichmann, On the duality condition for a Hermitian scalar field, J. Math. Phys. **16**, 985 (1975).

[31] J. J. Bisognano and E. H. Wichmann, On the duality condition for quantum fields, J. Math. Phys. **17**, 303 (1976).

[32] T. Mendes-Santos, G. Giudici, M. Dalmonte, and M. A. Rajabpour, Entanglement Hamiltonian of quantum critical chains and conformal field theories, Phys. Rev. B **100**, 155122 (2019).

[33] I. Bloch, Ultracold quantum gases in optical lattices, Nat. Phys. **1**, 23 (2005).

[34] M. Lewenstein, A. Sanpera, V. Ahufinger, B. Damski, A. Sen (De), and U. Sen, Ultracold atomic gases in optical lattices: Mimicking condensed matter physics and beyond, Adv. Phys. **56**, 243 (2007).

[35] I. Bloch, Quantum coherence and entanglement with ultracold atoms in optical lattices, Nature (London) **453**, 1016 (2008).

[36] I. Bloch, J. Dalibard, and S. Nascimbène, Quantum simulations with ultracold quantum gases, Nat. Phys. **8**, 267 (2012).

[37] C. Gross and I. Bloch, Quantum simulations with ultracold atoms in optical lattices, Science **357**, 995 (2017).

[38] A. G. Volosniev, D. V. Fedorov, A. S. Jensen, M. Valiente, and N. T. Zinner, Strongly interacting confined quantum systems in one dimension, Nat. Commun. **5**, 5300 (2014).

[39] F. Deuretzbacher, D. Becker, J. Bjerlin, S. M. Reimann, and L. Santos, Quantum magnetism without lattices in strongly interacting one-dimensional spinor gases, Phys. Rev. A **90**, 013611 (2014).

[40] L. Yang, L. Guan, and H. Pu, Strongly interacting quantum gases in one-dimensional traps, Phys. Rev. A **91**, 043634 (2015).

[41] P. Massignan, J. Levinsen, and M. M. Parish, Magnetism in Strongly Interacting One-Dimensional Quantum Mixtures, Phys. Rev. Lett. **115**, 247202 (2015).

[42] H. Moritz, T. Stöferle, K. Güenter, M. Köhl, and T. Esslinger, Confinement Induced Molecules in a 1D Fermi Gas, Phys. Rev. Lett. **94**, 210401 (2005).

[43] Y.-A. Liao, A. S. C. Rittner, T. Paprotta, W. Li, G. B. Partridge, R. G. Hulet, S. K. Baur, and E. J. Mueller, Spin-imbalance in a one-dimensional Fermi gas, Nature (London) **467**, 567 (2010).

[44] G. Zürn, F. Serwane, T. Lompe, A. N. Wenz, M. G. Ries, J. E. Bohn, and S. Jochim, Fermionization of Two Distinguishable Fermions, Phys. Rev. Lett. **108**, 075303 (2012).

[45] G. Pagano, M. Mancini, G. Cappellini, P. Lombardi, F. Schäfer, H. Hu, X.-J. Liu, J. Catani, C. Sias, M. Inguscio, and L. Fallani, A one-dimensional liquid of fermions with tunable spin, Nat. Phys. **10**, 198 (2014).

[46] T. A. Hilker, G. Salomon, F. Grusdt, A. Omran, M. Boll, E. Demler, I. Bloch, and C. Gross, Revealing hidden antiferromagnetic correlations in doped Hubbard chains via string correlators, Science **357**, 484 (2017).

[47] B. Paredes, A. Widera, V. Murg, O. Mandel, S. Folling, I. Cirac, G. V. Shlyapnikov, T. W. Hansch, and I. Bloch, Tonks-Girardeau gas of ultracold atoms in an optical lattice, Nature (London) **429**, 277 (2004).

[48] T. Kinoshita, T. Wenger, and D. S. Weiss, Observation of a one-dimensional Tonks-Girardeau gas, Science **305**, 1125 (2004).

[49] S. Trotzky, P. Cheinet, S. Fölling, M. Feld, U. Schnorrberger, A. M. Rey, A. Polkovnikov, E. A. Demler, M. D. Lukin, and I. Bloch, Time-resolved observation and control of superexchange interactions with ultracold atoms in optical lattices, Science **319**, 295 (2008).

[50] E. Haller, M. Gustavsson, M. J. Mark, J. G. Danzl, R. Hart, G. Pupillo, and H.-C. Nägerl, Realization of an excited, strongly correlated quantum gas phase, Science **325**, 1224 (2009).

[51] E. Haller, R. Hart, M. J. Mark, J. G. Danzl, L. Reichsollner, M. Gustavsson, M. Dalmonte, G. Pupillo, and H.-C. Nagerl, Pinning quantum phase transition for a Luttinger liquid of strongly interacting bosons, Nature (London) **466**, 597 (2010).

[52] S. Murmann, F. Deuretzbacher, G. Zürn, J. Bjerlin, S. M. Reimann, L. Santos, T. Lompe, and S. Jochim, Antiferromagnetic Heisenberg Spin Chain of a Few Cold Atoms in a One-Dimensional Trap, Phys. Rev. Lett. **115**, 215301 (2015).

[53] H. Casini, M. Huerta, and R. C. Myers, Towards a derivation of holographic entanglement entropy, J. High Energy Phys. 05 (2011) 036.

[54] A. G. Volosniev, D. Petrosyan, M. Valiente, D. V. Fedorov, A. S. Jensen, and N. T. Zinner, Engineering the dynamics of effective spin-chain models for strongly interacting atomic gases, Phys. Rev. A **91**, 023620 (2015).

[55] R. E. Barfknecht, A. Foerster, and N. T. Zinner, Dynamics of spin and density fluctuations in strongly interacting few-body systems, Sci. Rep. **9**, 15994 (2019).

[56] N. Loft, L. Kristensen, A. Thomsen, A. Volosniev, and N. Zinner, CONAN—The cruncher of local exchange coefficients for strongly interacting confined systems in one dimension, Comput. Phys. Commun. **209**, 171 (2016).

[57] F. Deuretzbacher, D. Becker, and L. Santos, Momentum distributions and numerical methods for strongly interacting one-dimensional spinor gases, Phys. Rev. A **94**, 023606 (2016).

[58] G. Veeravalli, E. Kuhnle, P. Dyke, and C. J. Vale, Bragg Spectroscopy of a Strongly Interacting Fermi Gas, Phys. Rev. Lett. **101**, 250403 (2008).

[59] Y. Zhang, L. Vidmar, and M. Rigol, Information measures for a local quantum phase transition: Lattice fermions in a one-dimensional harmonic trap, Phys. Rev. A **97**, 023605 (2018).

[60] J. Dubail, J.-M. Stéphan, J. Viti, and P. Calabrese, Conformal field theory for inhomogeneous one-dimensional quantum systems: The example of non-interacting fermi Gases, SciPost Phys. **2**, 002 (2017).

[61] E. Tonni, J. Rodríguez-Laguna, and G. Sierra, Entanglement Hamiltonian and entanglement contour in inhomogeneous 1D critical systems, J. Stat. Mech.: Theory Exp. (2018) 043105.

[62] S. Murciano, P. Ruggiero, and P. Calabrese, Entanglement and relative entropies for low-lying excited states in inhomogeneous one-dimensional quantum systems, J. Stat. Mech.: Theory Exp. (2019) 034001.

[63] Y. Zhang, L. Vidmar, and M. Rigol, Information measures for local quantum phase transitions: Lattice bosons in a one-dimensional harmonic trap, Phys. Rev. A **100**, 053611 (2019).

[64] J. Levinsen, P. Massignan, G. M. Bruun, and M. M. Parish, Strong-coupling ansatz for the one-dimensional Fermi gas in a harmonic potential, Sci. Adv. **1**, e1500197 (2015).

[65] L. Yang and H. Pu, Bose-Fermi mapping and a multibranch spin-chain model for strongly interacting quantum gases in one dimension: Dynamics and collective excitations, Phys. Rev. A **94**, 033614 (2016).

[66] M. Mancini, G. Pagano, G. Cappellini, L. Livi, M. Rider, J. Catani, C. Sias, P. Zoller, M. Inguscio, M. Dalmonte, and L. Fallani, Observation of chiral edge states with neutral fermions in synthetic Hall ribbons, Science **349**, 1510 (2015).

[67] C. Chin, R. Grimm, P. Julienne, and E. Tiesinga, Feshbach resonances in ultracold gases, Rev. Mod. Phys. **82**, 1225 (2010).

[68] M. Olshanii, Atomic Scattering in the Presence of an External Confinement and a Gas of Impenetrable Bosons, Phys. Rev. Lett. **81**, 938 (1998).

[69] A. J. A. James, W. D. Goetze, and F. H. L. Essler, Finite-temperature dynamical structure factor of the Heisenberg-Ising chain, Phys. Rev. B **79**, 214408 (2009).

[70] N. Fabbri, M. Panfil, D. Clément, L. Fallani, M. Inguscio, C. Fort, and J.-S. Caux, Dynamical structure factor of one-dimensional Bose gases: Experimental signatures of beyond-Luttinger-liquid physics, Phys. Rev. A **91**, 043617 (2015).

[71] Y.-R. Shu, M. Dupont, D.-X. Yao, S. Capponi, and A. W. Sandvik, Dynamical properties of the $s = \frac{1}{2}$ random Heisenberg chain, Phys. Rev. B **97**, 104424 (2018).

[72] L. Fallani (private communication, 2020).

[73] P. Kim, H. Katsura, N. Trivedi, and J. H. Han, Entanglement and corner Hamiltonian spectra of integrable open spin chains, Phys. Rev. B **94**, 195110 (2016).

[74] L. Yang and X. Cui, Effective spin-chain model for strongly interacting one-dimensional atomic gases with an arbitrary spin, Phys. Rev. A **93**, 013617 (2016).

[75] E. K. Laird, Z.-Y. Shi, M. M. Parish, and J. Levinsen, SU(N) fermions in a one-dimensional harmonic trap, Phys. Rev. A **96**, 032701 (2017).

[76] ITensor Library (version 3.1), http://itensor.org.

[77] E. H. Lieb and W. Liniger, Exact analysis of an interacting Bose gas, I. The general solution and the ground state, Phys. Rev. **130**, 1605 (1963).

[78] F. Deuretzbacher, K. Fredenhagen, D. Becker, K. Bongs, K. Sengstock, and D. Pfannkuche, Exact Solution of Strongly Interacting Quasi-One-Dimensional Spinor Bose Gases, Phys. Rev. Lett. **100**, 160405 (2008).

[79] M. Girardeau, Relationship between systems of impenetrable bosons and fermions in one dimension, J. Math. Phys. **1**, 516 (1960).

[80] A. Kleine, C. Kollath, I. P. McCulloch, T. Giamarchi, and U. Schollwöck, Spin-charge separation in two-component Bose gases, Phys. Rev. A **77**, 013607 (2008).